Available online at www.sciencedirect.com

ScienceDirect

journal homepage: www.elsevier.com/locate/he

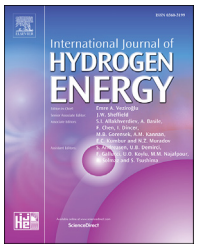

Fe-Cu coated nickel mesh usage as cathode catalyst for hydrogen evolution reaction

Esra Telli[*], *Denizhan Özer*

Osmaniye Korkut Ata University, Engineering Faculty, Energy Systems Engineering Department, 80000 Osmaniye, Turkey

ARTICLE INFO

Article history:
Received 4 January 2018
Received in revised form
12 February 2018
Accepted 27 February 2018
Available online 19 March 2018

Keywords:
Hydrogen evolution
Nickel mesh
Cathode catalyst

ABSTRACT

Nickel mesh electrodes were used as the working electrode. Iron and copper were electrochemically deposited on the nickel mesh in different amounts. When electrochemical coatings had been carried out, different currents were passed from the circuit at different times and coatings were accumulated at constant load. The prepared electrodes called as FexCux, FexCu3x and FexCu9x and these electrodes have been used for hydrogen evolution reaction (HER). The surface morphologies were investigated by scanning electron microscopy. The HER activity is assessed by recording cathodic current–potential curves, cyclic voltammetry, electrochemical impedance spectroscopy. The results show that FexCu9x catalysts have a compact and porous structure as well as good electrocatalytic activity for the HER in alkaline media.

Introduction

Energy is the most important notion of the 21st century [1]. With the decline of primary energy resources over time and the increase in energy demand, the search for different energy sources has increased [2]. In addition, scientists have turned to green energy sources because of the global warming and climate change that has begun in the world. Among green energy sources, hydrogen is a species with a high potential for sustainable energy [3,4]. Hydrogen is one of the most perspective fuels of energy. The basic advantages of hydrogen are high calorie value and abundant in the environment [2]. Furthermore, the fact that the energy density of hydrogen is high and it is a good energy carrier increases the preference of hydrogen [5–7]. Hydrogen can be produced by a variety of methods such as coal gasification, thermolysis, thermal water separation, hydrocarbon steam reforming, biomass pyrolysis, photolysis and electrolysis [8,9]. Because electrolysis is simple and efficient, it is the most used method to produce hydrogen [9–11]. Electrolysis is the decomposition of water into components electrochemically. The hydrogen evolution reaction (HER) formed by electrocatalytic separation of water can provide a sustainable energy support for the future. However, there are problems such as resource constraint and high cost because noble metals are used in this technique [2]. Cathodes containing platinum are often used as catalysts in the hydrogen evolution reaction. However, it is not very preferred for use due to platinum poisoning problem [12]. For this reason, easy to find and cheap materials should be developed to use as electrocatalyst to produce hydrogen. There are many studies related to electrocatalysis development [13–18]. The desired properties of the electrocatalysts are low overvoltage, high exchange current density, high surface area and long-time stability [19–22].

* *Corresponding author.*
E-mail address: esratelli@osmaniye.edu.tr (E. Telli).
https://doi.org/10.1016/j.ijhydene.2018.02.183

Nickel and its alloys have intrinsic electrocatalytic properties for hydrogen evolution reaction with suitable corrosion resistance in alkaline environment [23–25]. Nickel-supported electrocatalysts have high activity and low cost compared to other transition metals [26]. As the electrocatalyst, different types of nickel such as Ni-based alloys, Ni-based composites, Ni foam and Ni mesh can be used. Ni mesh is produced for applications such as fuel cells, cathode ray tube, sonic control and UV filtration. In addition, the flexibility of the Ni mesh allows it to be shaped into different forms and placed closer to the anode to reduce ohmic loss [27]. The Ni mesh is used as a current collector especially in different applications [28–30]. For instance, in pyrolysis of ethane [31] and oxidation [32], acetylene pyrolysis [33], methane oxidation [34], direct ethanol fuel cell [35] and solid oxide fuel cells [36]. Iron, copper metals which have high abundance and are not expensive and these alloys, are used as electrocatalysts in different forms [37–50]. Their performance has been well studied but there is no study about nickel mesh supporting material with these alloys.

In this study, unlike the studies in the literature, we aimed to obtain a material with high catalytic properties by co-depositing iron and copper on nickel mesh at different current densities for use in HER. The surface characterization of prepared electrode was done by scanning electron microscopy (SEM) technique. The electrocatalytic activity of the developed electrode for HER is evaluated in 1.0 M KOH solution using polarization curves and the electrochemical impedance spectroscopy (EIS).

Experimental

Nickel mesh electrodes with a thickness of 1.6 mm and a width of 1 cm and a height of 1 cm were used as the based material. Nickel mesh electrode was purchased from MTI Corporation. Its density is 346 g/m^2 and 80–110 Pores per Inch. Average hole diameters about 0.25 mm. Nickel mesh electrodes were awaited in the ultrasonic bath in acetone for half an hour before the electrochemical deposition step to clean the oil and dirt layer on the surface. Then, they were kept in the ultrasonic bath in a 3.0 M HCl acid solution during 1 h to activate the surface. The prepared nickel mesh electrodes were removed from the acid and then washed with ultrapure water. They were immersed in an iron-copper bath to make electrochemical coatings.

The iron copper bath composition is as follows.

Copper bath: 27.72% $CuSO_4 \cdot 5H_2O$, 1.25% H_3BO_3 (w/w) [51].

Iron bath: 30.86% $FeSO_4 \cdot 7H_2O$ and 1.25% H_3BO_3 (w/w) [17].

For each coating process, copper and iron baths are mixed in different volumes (Fe: Cu; 50-50; 25–75 and 10–90 mL, respectively). The coating operations were carried out using the direct current source (TT Technic-YH-303D). Platinum anode with a surface area of 2 cm^2 was used as counter electrode. Iron - Copper was coated on the nickel mesh by a constant charge of 4.350 C to the electrolysis system applying different currents (29, 58, 87, 116 and 145 mA). After deposition, the electrodes were rinsed with distilled water to remove residues of bath chemicals.

The electrochemical characterizations of electrodes were analyzed by EIS, CV, and potentiodynamic polarization techniques. Ag/AgCl and Pt (2 cm^2 surface area) were used as a reference and counter electrodes, respectively. CV analysis was determined at 100 mV s^{-1} scan rate. EIS experiments were obtained by a range of frequencies from 10^6 to 0.01 Hz at 5 mV amplitude. Moreover, potentiodynamic polarization plots were analyzed at 1 mV s^{-1} scan rate at cathodic direction. All experiments were done in 1.00 M KOH solution at room temperature.

SEM (scanning electron microscopy) (FEI Quanta 650 Field Emission SEM) and EDX (energy-dispersive X-ray spectroscopy) (EDAX octane plus) analysis were performed to determine the surface morphology of the coated electrodes. Cyclic voltammetry (CV), electrochemical impedance spectroscopy (EIS) and potentiodynamic polarization curves analysis were performed with the potentiostat-galvanostat device (Gamry Interface 1000) for the electrochemical characterization of the electrodes.

Results and discussion

The SEM images of the coatings made at 87 mA for 100 s are given in Fig. 1. When the SEM images are examined, the formation of copper metal clusters is observed with the increase of the proportion of copper in the cover. The effect of iron in the 1:1 ratio coating is seen. However, with the increase in the amount of copper, iron coatings remained between the copper metals, and this increased the catalytic activity of the alloy electrode.

The EDAX analysis results are shown in Tables 1 and 2. Applying currents of different magnitudes seems to affect the proportion of metals deposited on the electrode surface. Table 2 shows that the amount of copper deposited is high, even when the amounts of copper and iron in the coating bath are the same. It is understood from the EDAX analysis that this is a competing accumulation. The movement of copper ions to the electrode surface is faster than that of iron ions. It is seen that the amount of copper deposited on the surface of the electrode increases with the increase of the amount of added copper.

Fig. 2 shows the CVs of FexCux, FexCu3x and FexCu9x on Nickel mesh support in 1.00 M KOH solution at 298 K. CV peaks are related to Fe/Fe^{2+} (−0.40 V), Cu^+/Cu^{2+} (−0.10 V) and Ni^{2+}/Ni^{3+} (0.53 V) oxidation. The peak of Ni^{2+}/Ni^{3+} transition which is occurred by Ni-mesh based material are dominated by Cu/Cu^{2+} peak at FexCu9x electrode. The cathodic peaks correspond to the Ni^{3+}/Ni^{2+}, Cu^{2+}/Cu^+ and Fe/Fe^{2+} reduction, respectively. In Fig. 2, anodic and cathodic peak intensity at the CVs of the FexCux, FexCu3x and FexCu9x electrodes increase with increasing copper composition on the electrode. Ni^{2+}/Ni^{3+}oxidation peak current value of the FexCu9x electrode is higher than other electrodes.

The Nyquist (a) and Bode (b) curves of FexCux, FexCu3x and FexCu9x electrodes in 1.0 M KOH are seen in Fig. 3. The EIS results were obtained for FexCux, FexCu3x and FexCu9x electrodes as a cathode material with regards to potential usage for hydrogen evolution reaction (HER) in alkaline

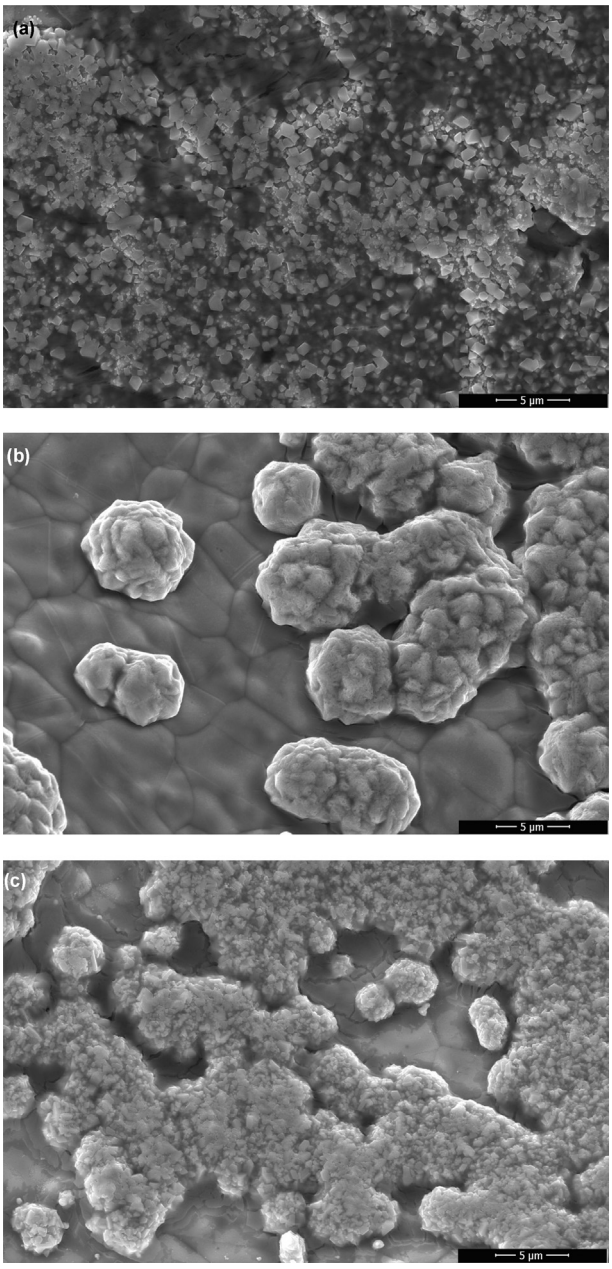

Fig. 1 – SEM micrographs of FexCux (a), FexCu3x (b) and FexCu9x (c) electrodes.

Table 1 – EDAX results of FexCu9x electrodes obtained at different current.

% Weight – Fe_xCu_{9x}	O	Fe	Ni	Cu
29 mA	5,76	1,33	51,68	41,22
58 mA	7,17	1,17	53,83	29,74
87 mA	4,1	0,85	52,12	42,93
121 mA	3	0,7	54,48	41,82
151 mA	8,43	2,28	39,09	50,21

Table 2 – EDAX results of FexCux, FexCu3x and FexCu9x electrodes.

	O	Fe	Ni	Cu
% Weight – Fe_xCu_x	18,2	11,54	34,83	35,42
% Weight – Fe_xCu_{3x}	6,15	0,85	46,78	38,66
% Weight – Fe_xCu_{9x}	4,1	0,85	52,12	42,93

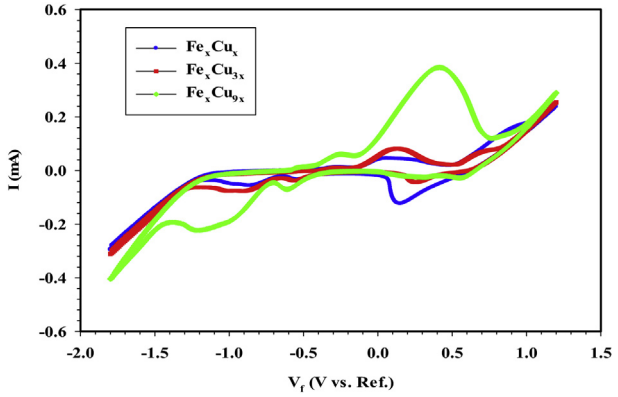

Fig. 2 – The cyclic voltammograms of FexCux, FexCu3x and FexCu9x electrodes obtained in 1.0 M KOH at 100 mV s^{-1} scan rate at 29 mA current and room temperature.

solution in the frequency range from 10^6 to 0.01 Hz. The equivalent circuit diagram used when the curves obtained for the HER process are fit is given in Fig. 3 as inset. In this diagram, Ru is the solution resistance, Rp is the polarization resistance consisting of the sum of the charge transfer resistance (Rct), the diffusion resistance (Rd) and the accumulation resistance (Ra) (Rp = Rct + Rd + Ra). In this system, there are two circuit elements that affect HER kinetics. One of them is Rp and the other is a constant phase element (Y_0). Since there is no equal amount of charge distribution on either side of the electrical double layer at a real interface, the circuit element is not a capacitance but a constant phase element. The provision of a single circuit element as the polarization resistance in the equivalent circuit shows that the coating on the surface is too small not to form a second resistance element. This single circuit (Rp) comprises both the nickel based material and the coating. All prepared electrodes have Nyquist diagrams with a depressed semi-circle in the high and middle frequency regions. In the low frequency range only the FexCux electrode contains the angular part originating from the diffusion layer resistance. This situation shows that for all electrodes the HER kinetics are controlled by diffusion. It is seen from Fig. 3a, the Nyquist plot of FexCu9x has the smallest capacitive loop. It is understood that FexCu9x has the lowest catalyst resistance and diffusion rate in comparison with FexCux and FexCu3x which indicate that it was more active from other electrodes for potential application of HER. The Bode plots support the Nyquist curves, which are seen in Fig. 3b. When the compared with the literature [52–56] containing Ni-based electrode Nyquist curve obtained from FexCu9x electrode, we have found that the resistance value of the electrode in terms of HER kinetics is lower.

Fig. 4 shows the cyclic voltammograms obtained in 1.0 M KOH at constant charge by using different currents with different periods (29 mA-300 s, 58 mA-150 s, 87 mA-100 s,

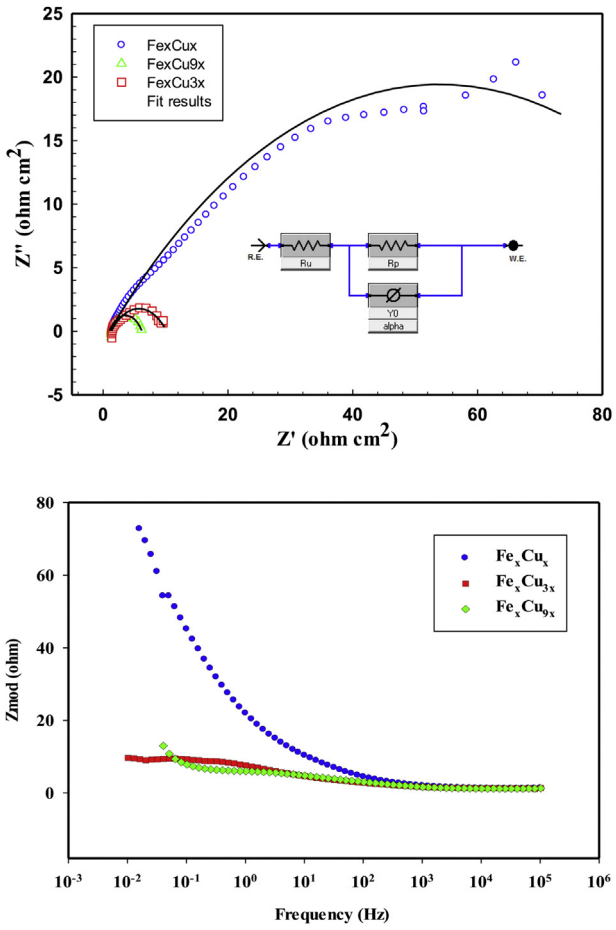

Fig. 3 – Nyquist (a) and Bode (b) plots for FexCux, FexCu3x and FexCu9x electrodes at room temperature. (inset: equivalent circuit diagram).

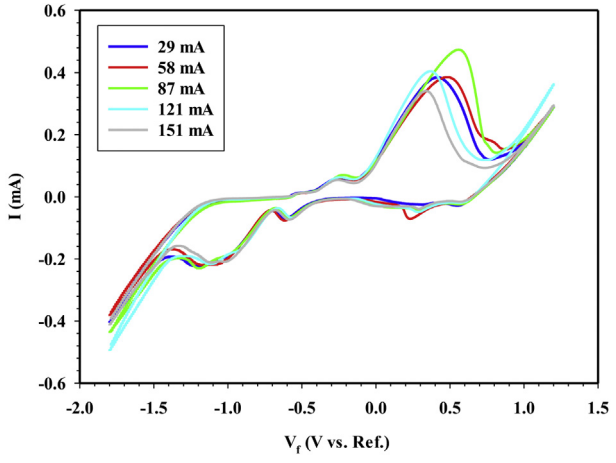

Fig. 4 – The cyclic voltammograms of FexCu9x electrodes obtained in 1.0 M KOH at 100 mV s^{-1} scan rate by applying different current (29, 58, 87, 116 and 145 mA) and room temperature.

116 mA-75 s and 145 mA-60 s) for the FexCu9x electrode. It is seen that the highest peak current is obtained at FexCu9x electrode which is electrodeposited by applying 87 mA current. Therefore, the current of 87 mA was chosen for the electrodeposition process. Electrodes which were deposited at 87 mA current were used for CV, EIS and potentiodynamic polarization techniques.

The potentiodynamic polarization curves of FexCux, FexCu3x and FexCu9x electrodes at the cathodic direction in 1.0 M KOH solution at 1 mV s^{-1} scan rate are seen in Fig. 5. As it can be seen in Figure, FexCu9x electrode has the lowest overpotential for HER in alkaline solution by comparison with FexCux and FexCu3x electrodes. Tafel constants were calculated by using potentiodynamic polarization curves from following equation [17].

$$\mu = a + b \log i \quad (1)$$

where μ (V) is overpotential, α (V) and b (V dec^{-1}) are called as Tafel constants and i (A cm^{-2}) is current density.

Tafel slope should be clarified the rate determining step (rds). When the tafel slopes assume the following values, the corresponding rds are as in Table 3 [17]. In alkaline solutions, HER on a metallic electrocatalyst can follow either the Volmer-Heyrovsky-Tafel mechanism (Eqs. (2)–(4)) [57],

$$M + H_2O + e^- \rightleftharpoons MH_{ads} + OH^-_{ads} \quad (Volmer\ step) \quad (2)$$

$$MH_{ads} + H_2O + e^- \rightleftharpoons H_2 + M + OH^-_2 \quad (Heyrovsky\ step) \quad (3)$$

$$MH_{ads} + MH_{ads} \rightleftharpoons H_2 + 2M \quad (Tafel\ step) \quad (4)$$

The calculated Tafel constant of FexCu9x from potentiodynamic polarization curve is 265 mV dec^{-1}. The measured Tafel slope increased according to 120 mV dec^{-1}. The reason of this phenomenon should be claimed that the oxide film occurred on iron. The formation of oxide film could be deviated from ideal Tafel slope. So, Tafel slope value should be increased. However, the reaction mechanism does not change [58]. Moreover, the linear Tafel curves at negative potentials

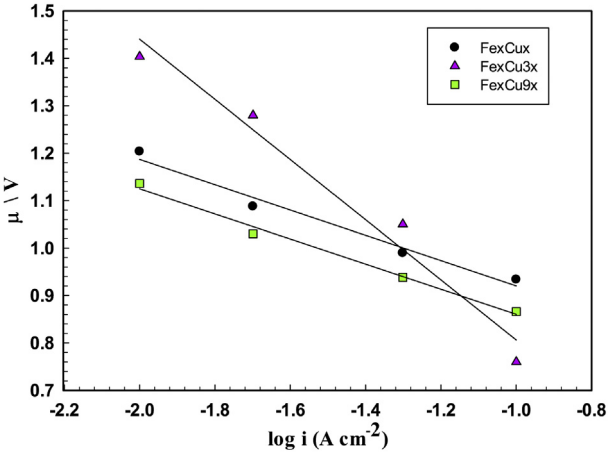

Fig. 5 – The cathodic polarization curves of FexCux, FexCu3x and FexCu9x in 1.0 M KOH solution at 1 mV s^{-1} scan rate at room temperature.

Table 3 – rds and Tafel slope relation.

Tafel Slope (V dec^{-1})	rds
120	Volmer
40	Heyrovsky
30	Tafel

show that HER mechanism is taken place by Volmer reaction followed Heyrovsky step.

Conclusions

The FexCux, FexCu3x and FexCu9x electrodes were prepared and analyzed for hydrogen evolution reaction.

- The SEM images show that the different amount of copper has changed the surface area.
- According to the CV results, the current of FexCu9x electrode is higher than FexCu3x and FexCux electrodes.
- When the investigated HER kinetic from EIS results of prepared electrodes is seen that the FexCu9x electrode has the lowest resistance. This result was compared with literature and the observed results were higher than FexCu9x electrode.
- The overpotential of FexCu9x electrode obtained by potentiodynamic polarization curves was lower than other electrodes and the HER mechanism was determined as Volmer-Heyrovsky from potentiodynamic polarization curves.

In view of these results, FexCu9x electrode is suitable for use as a catalyst for hydrogen production.

Acknowledgements

This study has been financially supported by Osmaniye Korkut Ata University research fund. The authors are greatly thankful to Osmaniye Korkut Ata University research fund (Project Number: OKÜBAP-2015-PT3-007) and Çukurova University. The authors would like to especially thanks to Gülfeza Kardaş and Murat Farsak for help.

REFERENCES

[1] Zhang KY, Xiao W, Li JY, Liu JG, Yan CW. Two-step preparation of porous nickel-sulfur electrode for hydrogen evolution in alkaline water electrolysis. Electrochim Acta 2017;228:422–7.
[2] Streckova M, Mudra E, Orinakova R, Markusova-Buckova L, Sebek M, Kovalcikova A, et al. Nickel and nickel phosphide nanoparticles embedded in electrospun carbon fibers as favourable electrocatalysts for hydrogen evolution. Chem Eng J 2016;303:167–81.
[3] Bockris JOM. The origin of ideas on a Hydrogen Economy and its solution to the decay of the environment. Int J Hydrogen Energy 2002;27:731–40.
[4] Sandeep KC, Kamath S, Mistry K, Kumar MS, Bhattacharya SK, Bhanja K, et al. Experimental studies and modeling of advanced alkaline water electrolyser with porous nickel electrodes for hydrogen production. Int J Hydrogen Energy 2017;42:12094–103.
[5] Yoo J, Bang Y, Han SJ, Park S, Song JH, Song IK. Hydrogen production by tri-reforming of methane over nickel-alumina aerogel catalyst. J Mol Catal A Chem 2015;410:74–80.
[6] Lee CH, Mun S, Lee KB. Application of multisection packing concept to sorption-enhanced steam methane reforming reaction for high-purity hydrogen production. J Power Sources 2015;281:158–63.
[7] Holladay JD, Hu J, King DL, Wang Y. An overview of hydrogen production technologies. Catal Today 2009;139:244–60.
[8] Navarro RM, Pena MA, Fierro JLG. Hydrogen production reactions from carbon feedstocks: fossils fuels and biomass. Chem Rev 2007;107:3952–91.
[9] Miles MH. Evaluation of electrocatalysts for water electrolysis in alkaline solutions. J Electroanal Chem Interfacial Electrochem 1975;60:89–96.
[10] Lupi C, Dell'Era A, Pasquali M. Nickel–cobalt electrodeposited alloys for hydrogen evolution in alkaline media. Int J Hydrogen Energy 2009;34:2101–6.
[11] Nivetha R, Santhosh C, Kollu P, Jeong SK, Bhatnagar A, Grace AN. Cobalt and nickel ferrites based graphene nanocomposites for electrochemical hydrogen evolution. J Magn Magn Mater 2017;448:165–71.
[12] Mitov M, Chorbadzhiyska E, Nalbandian L, Hubenova Y. Nickel-based electrodeposits as potential cathode catalysts for hydrogen production by microbial electrolysis. J Power Sources 2017;356:467–72.
[13] Chen Y-Q, Zhang J-F, Lei W, Hu W-B, Lei L, Zhong C, et al. Effect of nickel phosphide nanoparticles crystallization on hydrogen evolution reaction catalytic performance. Trans Nonferrous Metals Soc China 2017;27:369–76.
[14] Chen WF, Sasaki K, Ma C, Frenkel AI, Marinkovic N, Muckerman JT, et al. Hydrogen-evolution catalysts based on non-noble metal nickel–molybdenum nitride nanosheets. Angew Chem Int Ed 2012;51:6131–5.
[15] Huang L, Yang F-Z, Xu S-K, Zhou S-M. Studies of structure and electrocatalytic hydrogen evolution on electrodeposited nanocrystalline Ni-Mo alloy electrodes. Trans IMF 2001;79:136–9.
[16] Farsak M, Kardaş G. Enhanced electrocatalytic efficiency of C/MWNTs for methanol oxidation using Ni deposited on MWNTs. Turk J Chem 2015;39:813.
[17] Farsak M, Telli E, Yüce AO, Kardaş G. The noble metal loading binary iron–zinc electrode for hydrogen production. Int J Hydrogen Energy 2017;42:6455–61.
[18] Telli E, Farsak M, Kardaş G. Investigation of noble metal loading CoWZn electrode for HER. Int J Hydrogen Energy 2017;42:23260–7.
[19] Kalaiyarasan G, Aswathi K, Joseph J. Formation of nanoporous NiS films from electrochemically modified GC surface with nickel hexacyanoferrate film and its performance for the hydrogen evolution reaction. Int J Hydrogen Energy 2017;42:22866–76.
[20] Darband GB, Aliofkhazraei M, Rouhaghdam AS. Nickel nanocones as efficient and stable catalyst for electrochemical hydrogen evolution reaction. Int J Hydrogen Energy 2017;42:14560–5.
[21] Shervedani RK, Lasia A. Study of the hydrogen evolution reaction on Ni-Mo-P electrodes in alkaline solutions. J Electrochem Soc 1998;145:2219–25.
[22] Kubisztal J, Budniok A, Lasia A. Study of the hydrogen evolution reaction on nickel-based composite coatings containing molybdenum powder. Int J Hydrogen Energy 2007;32:1211–8.

[23] Burchardt T. The hydrogen evolution reaction on NiPx alloys. Int J Hydrogen Energy 2000;25:627–34.
[24] Kedzierzawski P, Oleszak D, Janik-Czachor M. Hydrogen evolution on hot and cold consolidated Ni–Mo alloys produced by mechanical alloying. Mater Sci Eng A 2001;300:105–12.
[25] Gong M, Wang D-Y, Chen C-C, Hwang B-J, Dai H. A mini review on nickel-based electrocatalysts for alkaline hydrogen evolution reaction. Nano Res 2016;9:28–46.
[26] Zamzuri NH, Mat R, Amin NAS, Talebian-Kiakalaieh A. Hydrogen production from catalytic steam reforming of glycerol over various supported nickel catalysts. Int J Hydrogen Energy 2017;42:9087–98.
[27] Kadier A, Simayi Y, Chandrasekhar K, Ismail M, Kalil MS. Hydrogen gas production with an electroformed Ni mesh cathode catalysts in a single-chamber microbial electrolysis cell (MEC). Int J Hydrogen Energy 2015;40:14095–103.
[28] Peng T, Wang H, Yi H, Jing Y, Sun P, Wang X. $Co(OH)_2$ nanosheets coupled with CNT arrays grown on Ni mesh for high-rate asymmetric supercapacitors with excellent capacitive behavior. Electrochim Acta 2015;176:77–85.
[29] Yamauchi K, Nogami S, Martinez-de la Cruz G, Hirayama B, Shimizu Y, Kumamoto H, et al. Timed-release system for periosteal expansion osteogenesis using NiTi mesh and absorbable material in the rabbit calvaria. J Cranio Maxillofacial Surg 2016;44:1366–72.
[30] Kim M, Lee J-Y, Kwon S-C, Kim D, Kim I-G, Choi Y. Application of small angle neutron scattering to analyze precision nickel mesh for electro-magnetic interference shielding formed by continuous electroforming technique. Phys B Condens Matter 2006;385:914–6.
[31] Lee WJ, Li C-Z. Coke formation and reaction pathways of catalyst-surface-generated radicals during the pyrolysis of ethane using Ni mesh catalyst. Appl Catal A Gen 2007;316:90–9.
[32] Syed-Hassan SSA, Lee WJ, Li C-Z. Positive and negative catalytic effects of a nickel mesh catalyst for the partial oxidation of ethane. Chem Eng J 2009;147:307–15.
[33] Lee WJ, Li C-Z. Opposite effects of gas flow rate on the rate of formation of carbon during the pyrolysis of ethane and acetylene on a nickel mesh catalyst. Carbon 2008;46:1208–17.
[34] Quah EB, Li C-Z. Roles of desorbed radicals and reaction products during the oxidation of methane using a nickel mesh catalyst. Appl Catal A Gen 2004;258:63–71.
[35] Basu S, Agarwal A, Pramanik H. Improvement in performance of a direct ethanol fuel cell: effect of sulfuric acid and Ni-mesh. Electrochem Commun 2008;10:1254–7.
[36] Li T, Wu Z, Li K. A dual-structured anode/Ni-mesh current collector hollow fibre for micro-tubular solid oxide fuel cells (SOFCs). J Power Sources 2014;251:145–51.
[37] Xin Z-J, Liu S, Li C-B, Lei Y-J, Xue D-X, Gao X-W, et al. Hydrogen production in a neutral aqueous solution with a water-soluble copper complex. Int J Hydrogen Energy 2017;42:4202–7.
[38] Canavesio C, Nassini HE, Bohé AE. Evaluation of an iron-chlorine thermochemical cycle for hydrogen production. Int J Hydrogen Energy 2015;40:8620–32.
[39] Chiron F-X, Patience GS. Kinetics of mixed copper–iron based oxygen carriers for hydrogen production by chemical looping water splitting. Int J Hydrogen Energy 2012;37:10526–38.
[40] Naterer GF, Suppiah S, Rosen MA, Gabriel K, Dincer I, Jianu OA, et al. Advances in unit operations and materials for the CuCl cycle of hydrogen production. Int J Hydrogen Energy 2017;42:15708–23.
[41] Mohanraj S, Anbalagan K, Rajaguru P, Pugalenthi V. Effects of phytogenic copper nanoparticles on fermentative hydrogen production by Enterobacter cloacae and Clostridium acetobutylicum. Int J Hydrogen Energy 2016;41:10639–45.
[42] Wang ZL, Naterer GF, Gabriel KS, Gravelsins R, Daggupati VN. Comparison of different copper–chlorine thermochemical cycles for hydrogen production. Int J Hydrogen Energy 2009;34:3267–76.
[43] Balta MT, Dincer I, Hepbasli A. Comparative assessment of various chlorine family thermochemical cycles for hydrogen production. Int J Hydrogen Energy 2016;41:7802–13.
[44] Naterer GF, Gabriel K, Wang ZL, Daggupati VN, Gravelsins R. Thermochemical hydrogen production with a copper–chlorine cycle. I: oxygen release from copper oxychloride decomposition. Int J Hydrogen Energy 2008;33:5439–50.
[45] Li J, Pan X, Xu Y, Jia L, Yi X, Fang W. Synergetic effect of copper species as cocatalyst on $LaFeO_3$ for enhanced visible-light photocatalytic hydrogen evolution. Int J Hydrogen Energy 2015;40:13918–25.
[46] Pinilla JL, Utrilla R, Karn RK, Suelves I, Lázaro MJ, Moliner R, et al. High temperature iron-based catalysts for hydrogen and nanostructured carbon production by methane decomposition. Int J Hydrogen Energy 2011;36:7832–43.
[47] Chang C-Y, Wang C-H, Tseng C-J, Cheng K-W, Hourng L-W, Tsai B-T. Self-oriented iron oxide nanorod array thin film for photoelectrochemical hydrogen production. Int J Hydrogen Energy 2012;37:13616–22.
[48] Perovic IM, Acimovic DD, Tasić GS, Karic SD, Lausevic PZ, Marčeta Kaninski MP, et al. Efficient hydrogen production using ternary Ni–Cu–Mo ionic activator. Int J Hydrogen Energy 2015;40:6270–5.
[49] Cao J-P, Fang T, Fu L-Z, Zhou L-L, Zhan S-Z. First mononuclear copper(II) electro-catalyst for catalyzing hydrogen evolution from acetic acid and water. Int J Hydrogen Energy 2014;39:13972–8.
[50] Mitov M, Chorbadzhiyska E, Rashkov R, Hubenova Y. Novel nanostructured electrocatalysts for hydrogen evolution reaction in neutral and weak acidic solutions. Int J Hydrogen Energy 2012;37:16522–6.
[51] Döner A, Solmaz R, Kardaş G. Fabrication and characterization of alkaline leached CuZn/Cu electrode as anode material for direct methanol fuel cell. Energy 2015;90:1144–51.
[52] Peng Q-X, Xue D, Zhan S-Z, Ni C-L. Visible-light-driven photocatalytic system based on a nickel complex over CdS materials for hydrogen production from water. Appl Catal B Environ 2017;219:353–61.
[53] Gultom NS, Abdullah H, Kuo D-H. Enhanced photocatalytic hydrogen production of noble-metal free Ni-doped Zn(O,S) in ethanol solution. Int J Hydrogen Energy 2017;42:25891–902.
[54] Bashiri R, Mohamed NM, Kait CF, Sufian S, Khatani M. Enhancing photoelectrochemical hydrogen production over Cu and Ni doped titania thin film: effect of calcination duration. J Environ Chem Eng 2017;5:3207–14.
[55] Torres C, Moreno B, Chinarro E, de Fraga Malfatti C. Nickel-polyaniline composite electrodes for hydrogen evolution reaction in alkaline media. Int J Hydrogen Energy 2017;42:20410–9.
[56] Chung Y-H, Gupta K, Jang J-H, Park HS, Jang I, Jang JH, et al. Rationalization of electrocatalysis of nickel phosphide nanowires for efficient hydrogen production. Nano Energy 2016;26:496–503.
[57] Vasić M, Čebela M, Pašti I, Amaral L, Hercigonja R, Santos DMF, et al. Efficient hydrogen evolution electrocatalysis in alkaline medium using Pd-modified zeolite X. Electrochim Acta 2018;259:882–92.
[58] Navarro-Flores E, Chong Z, Omanovic S. Characterization of Ni, NiMo, NiW and NiFe electroactive coatings as electrocatalysts for hydrogen evolution in an acidic medium. J Mol Catal A Chem 2005;226:179–97.